Simulation of dispersion of a power plant plume using an adaptive grid algorithm

R.K. Srivastava[a,*], D.S. McRae[b], M.T. Odman[c]

[a] *National Risk Management Research Laboratory, US Environmental Protection Agency, MD-65, 86 T.W. Alexander Drive, Research Triangle Park, NC 27711, USA*
[b] *Department of Mechanical and Aerospace Engineering, North Carolina State University, Raleigh, NC 27695-7910, USA*
[c] *Georgia Institute of Technology, School of Civil and Environmental Engineering, Atlanta, GA 30332-0512, USA*

Abstract

A new dynamic adaptive grid algorithm has been developed for use in air quality modeling. This algorithm uses a higher order numerical scheme—the piecewise parabolic method (PPM)—for computing advective solution fields; a weight function capable of promoting grid node clustering by moving grid nodes; and a conservative interpolation equation using PPM for redistributing the solution field after movement of grid nodes. Applications of the algorithm to a model problem, in which emissions from a point source disperse through the atmosphere in time, reflect that the algorithm is able to capture not only the regional ozone plume distribution, but also the small-scale plume structure near the source. In contrast, the small-scale plume structure was not captured in the corresponding static grid solution. Performance achieved in model problem simulations indicates that the algorithm has the potential to provide accurate air quality modeling solutions at costs that may be significantly less than those incurred in obtaining equivalent static grid solutions. © 2001 Elsevier Science Ltd. All rights reserved.

Keywords: Grid adaptation; Plume dispersion; Simulation of point source emissions; Air quality modeling; Simulation of reacting flow

1. Introduction

An air quality model (AQM) consists of coupled mathematical representations for atmospheric transport and chemistry processes. The interactions between these processes can significantly alter the spatial distributions of atmospheric species over time. For example, while the composition of a pollutant is changing due to chemical transformations, the concentration distribution of each species may be changing constantly due to various transport processes. Since the chemistry associated with air pollution is nonlinear, the accuracy of an AQM's predictions depends significantly on how well the gradients in the concentrations of various species can

be resolved. Averaging of reactant gradients over large cells may greatly underestimate local changes in concentrations, resulting in inaccurate estimates of the concentrations of reaction products. Therefore, to accurately predict air pollution, an AQM has to be able to adequately resolve the pertinent spatial scales. This can be achieved by varying the physical grid node spacing in an AQM to provide resolution where needed.

One approach to achieving increased local solution resolution involves using embedded Cartesian grids, or static nested grids, such as those described by Odman and Russell (1991) and Odman et al. (1997). This approach may be limited by: (1) the uncertainty in nested grid(s) placement(s) since pertinent locations may not be known a priori, (2) the loss in solution accuracy resulting from grid boundary interface problems, and (3) the inability to adjust rapidly to dynamic changes in solution resolution requirements. Another approach to

*Corresponding author. Tel.: +1-919-541-3444; fax: +1-919-541-0554.

E-mail address: srivastava.ravi@epa.gov (R.K. Srivastava).

achieving local solution resolution involves using dynamic adaptive grids. In principle, such grids would be continuous and would dynamically adjust to changing solution resolution requirements. Therefore, use of such grids would not be constrained by the limitations associated with the use of nested grids.

Several recent efforts examine the use of dynamic adaptive grids in atmospheric modeling. Dietachmayer and Droegemeier (1992) used a variational formulation of adaptive grid generation equations to compute solutions to test problems in atmospheric dynamics. Almgren et al. (1997) used a nested hierarchy of grids, with simultaneous refinement in both space and time, to simulate the release of a hot gas into the atmosphere. Skamarock and Klemp (1993) also used a hierarchical grid approach to model compressible atmospheric flow. Tomlin et al. (1997) investigated the use of an adaptive unstructured grid method in air quality modeling by solving various test problems.

This paper describes a new dynamic solution adaptive grid algorithm (DSAGA-PPM), which is suitable for use in AQMs. This new algorithm utilizes accurate solution procedures. Specifically, the DSAGA-PPM framework incorporates: (1) the *piecewise parabolic method* (PPM) developed by Collela and Woodward (1984) for computing the advective fluxes and the fluxes resulting from grid movement; (2) a new weight function formulation designed for reacting flows, and (3) a conservative solution field redistribution procedure.

DSAGA-PPM employs a constant number of grid nodes that, in two-dimensional space, partition a rectangular domain into $N \times M$ quadrilateral grid cells. The nodes move throughout the simulation but the grid structure remains the same. In other words, each interior node is still connected to the same four nodes (and boundary nodes to the same two or three nodes), but the length of the links and the area of the grid cells change. The movement of the nodes is controlled by a weight function whose value is proportional to the error in the solution. The nodes are clustered around regions where the weight function bears large values, thereby increasing the resolution where the error is large. Since the number of nodes is fixed, refinement of grid scales in regions of high interest is accompanied by coarsening in other regions where the weight function has smaller values. This yields a continuous multiscale grid where the scales change gradually. Unlike nested grids, there are no grid interfaces, which may introduce numerous difficulties due to the discontinuity of grid scales. The availability of computational resources determines the number of grid nodes that can be afforded in any AQM. By clustering grid nodes automatically in regions of interest, DSAGA-PPM makes efficient use of computational resources throughout the simulation.

The formulation of DSAGA-PPM and its ability to accurately describe the changes in concentration distributions due to advective transport and rapid nonlinear chemical transformations are described by Srivastava et al. (2000). However, in reality, distribution of pollutants in the atmosphere is affected by the nonlinear interactions between emissions from sources, advection, turbulent diffusion, and chemistry. Therefore, it is necessary to examine the ability of DSAGA-PPM to accurately simulate a problem with these interactions. Consequently, for this work, a model problem is designed in which emissions from a power plant lead to formation of ozone (O_3). Specifically, the power plant represents a point source of nitrogen oxides (NO_x) with a plume that can travel in the atmosphere for hundreds of miles. As the constituents of this plume move through the atmosphere, they interact with the background species to produce O_3. Tomlin et al. (1997) have used a similar model problem in their evaluation of an unstructured adaptive grid method.

2. DSAGA-PPM

DSAGA-PPM includes cell-centered finite volume procedures for advancing the solution of the governing system of equations in time using a non-uniform structured grid, for moving the grid nodes to region(s) requiring solution refinement, and for conservatively redistributing the solution field over the resulting adapted structured grid. These procedures are briefly described below. Details can be found in Srivastava et al. (2000) and Srivastava (1998).

2.1. Time advancement of the governing system

In an arbitrary, time-varying, spatial region $\Omega(t)$, located in the Euclidean space E^3 and bounded by $\partial \Omega(t)$, a spatial point is given by $\vec{X} = \{x, y, z\} \in \Omega(t)$. In $\Omega(t)$, the conservation of mass for each of the N chemical species $c_l\left(\vec{X}, t\right)$, $l = 1, ..., N$ is expressed as

$$\frac{\partial c_l}{\partial t} + \nabla \cdot (\vec{V} \cdot c_l) = \nabla \cdot (K \cdot \nabla c_l) + R_l(c_1, ..., c_N)$$
$$+ S_l(\vec{X}, t), \quad l = 1, ..., N, \qquad (1)$$

where c_l is the mass concentration of pollutant l (mass of pollutant l/volume of air), $\vec{V}(\vec{X}, t) = (u, v, w)$ is the specified wind field, K is a second order, diagonal, turbulent diffusivity tensor, R_l is the net generation of chemical species l by chemical reactions, and S_l is the rate of source addition for the chemical species l. Eq. (1) is referred to as *the atmospheric diffusion equation* (McRae et al., 1982) and constitutes the governing system for an AQM.

The atmospheric diffusion equation is solved with specified initial and boundary conditions. For each of species c_l, an initial distribution $c_l\left(\vec{X}, 0\right)$ is specified and

inhomogeneous mixed Neumann and Dirichlet boundary conditions are used. A discussion of the initial and boundary conditions can be found in Srivastava (1998).

In AQMs based on finite volume methods, the governing system consisting of the atmospheric diffusion equation (McRae et al., 1982) is usually advanced in time on static Cartesian grids with uniform spacing in the horizontal plane and non-uniform spacing in the vertical direction. However, in general, an adapted grid will not be uniform. Therefore in DSAGA-PPM, the solutions of the governing system need to be obtained on non-uniform grids. To facilitate this, a coordinate transformation is applied to the governing system to move from the physical domain expressed in Cartesian coordinates (x, y, z) to a computational domain expressed, in general curvilinear coordinates ξ^m; $m = 1, 2, 3$. The grid in these general curvilinear coordinates is assumed to be uniform and unit-spaced. This procedure allows the governing system to be solved on arbitrary physical grids (i.e., grids that are curved in space and aligned to shapes of existing solution features).

In ξ^m coordinates, the atmospheric diffusion equation is expressed as

$$\frac{\partial \hat{c}_l}{\partial t} + \frac{\partial \hat{E}_l^m}{\partial \xi^m} = \hat{R}_l + \hat{S}_l, \quad l = 1, \dots, N, \quad m = 1, 2, 3, \quad (2)$$

where

$$\hat{c}_l = c_l / J, \quad l = 1, \dots, N, \quad (3)$$

$$\hat{E}_l^m = \frac{\xi_x^m E_l + \xi_y^m F_l + \xi_z^m G_l}{J}, \quad l = 1, \dots, N, \quad (4)$$

$$\hat{R}_l = R_l(c_1, \dots, c_N) / J, \quad l = 1, \dots, N, \quad (5)$$

$$\hat{S}_l = S_l(\vec{X}, t) / J, \quad l = 1, \dots, N. \quad (6)$$

with $E_l = c_l u - K_{xx} \partial c_l / \partial x$, $F_l = c_l v - K_{yy} \partial c_l / \partial y$, and $G_l = c_l w - K_{zz} \partial c_l / \partial z$ for diagonal K with respect to Cartesian coordinates. The expressions for the Jacobian J and the metrics, ξ_x^m, ξ_y^m and ξ_z^m (the subscript denotes a partial derivative with respect to that Cartesian coordianate), of the transformation can be found in Anderson et al. (1984).

In general, Eq. (2) denotes a system of stiff partial differential equations because the time scales associated with typical chemical transformations are far smaller than those associated with transport due to advection and turbulent diffusion. Therefore, decoupling transport and chemistry and solving for these processes in sequential steps result in a more efficient computation of transport. As discussed in McRae et al. (1982), Eq. (2) is operator (or time) split to compute transport, chemistry, and source processes in sequential steps. This splitting is not unique and differs between AQMs. The

splitting sequence used in this work is

$$c_l(t + \Delta t) = L_{\text{chem}} L_{s_l} L_{\text{diff}} L_{\text{adv}} c_l(t), \quad l = 1, \dots, N, \quad (7)$$

$$c_l(t + 2\Delta t) = L_{\text{adv}} L_{\text{diff}} L_{s_l} L_{\text{chem}} c_l(t + \Delta t), \quad l = 1, \dots, N, \quad (8)$$

where, for example,

$$L_{\text{adv}} = \left[I + \Delta t \cdot J \frac{\partial}{\partial \xi^m} \left(\frac{\xi_x^m(-u) + \xi_y^m(-v) + \xi_z^m(-w)}{J} \right) \right]. \quad (9)$$

The expressions for other operators can be found in Srivastava et al. (2000).

The splitting defined by Eqs. (7) and (8) is symmetric and, as explained in McRae et al. (1982), is second order accurate.

In DSAGA-PPM, advection, turbulent diffusion, and chemistry operators have their own time steps Δt_{adv}, Δt_{diff} and Δt_{chem}, respectively. In general, $\Delta t_{\text{adv}} > \Delta t_{\text{diff}} > \Delta t_{\text{chem}}$. These processes are synchronized in time to ensure that they advance through the same time period in any solution step. The sequence of calculations is as follows. Following splitting (7) and (8), advection is computed first using Δt_{adv}. Next, diffusion is repeatedly applied using Δt_{diff} until the total time step for diffusion equals Δt_{adv}. Then, source emissions are calculated over a time period Δt_{adv}. Subsequently, chemistry is repeatedly applied using Δt_{chem} until the total time step for chemistry equals $2\Delta t_{\text{adv}}$. The internal time steps used by the chemistry solver are usually much smaller than $2\Delta t_{\text{adv}}$. This is necessary to obtain an accurate solution to the stiff system of equations that describe the nonlinear chemistry. Next, source emissions are calculated over a time period Δt_{adv}. Then, diffusion is repeatedly applied using Δt_{diff} until the total time step for diffusion equals Δt_{adv}. Finally, advection is computed using Δt_{adv}. This sequence of calculations advances the solution by $2\Delta t$ (or $2\Delta t_{\text{adv}}$). The details of calculation of Δt_{adv} and Δt_{diff} can be found in Srivastava (1998). It is worth noting that during a DSAGA-PPM simulation, Δt_{adv} and Δt_{diff} vary depending on the cell sizes of the adapting grid and that Δt_{chem} also varies due to changes in the stiffness of the chemical system.

In air quality simulations, mass conservation of species, monotonicity of the solution fields, and a high order of accuracy need to be maintained during numerical computations. The piecewise parabolic method (PPM)—a numerical scheme for computing advection—is monotonic, third order accurate for variable grid spacing, and conservative (Collela and Woodward, 1984 and Carpenter et al., 1990). Therefore, a time-split version of the PPM scheme is used in DSAGA-PPM to compute the advective fluxes. Moreover, advection is carefully formulated to eliminate the possibility of

introducing any spurious numerical sources (Srivastava et al., 2000).

The boundary conditions for species transport are termed either inflow or outflow, depending on the direction of flow at the grid boundary under consideration. In fluid flow situations, generally the species concentrations at inflow boundaries are known as a function of time. The outflow boundary conditions are generally not known and, therefore, need to be computed. In DSAGA-PPM, zero-concentration-gradient boundary conditions are used at outflow boundaries in the calculation of advection and turbulent diffusion.

Most emissions are released from either point locations (point sources) or area regions (area sources). In order to determine the incremental contribution from source emissions into a computational cell, consider a particular cell of base area A_b and uniform height $h(t)$. Given the mass emission rate E_l^P (e.g., kg/s) from a point source, the corresponding rate of change of concentration *in the cell containing this source* is given by

$$S_l^P = \frac{E_l^P}{h(t)A_b}. \tag{10}$$

In a DSAGA-PPM simulation, the specification of emission sources with respect to the grid may change, as the grid is adapted. For example, if before grid movement the grid cell m contains a point source, after grid movement cell $n \neq m$ may contain the same point source. Moreover, if a point source was located within a cell before grid movement, after grid movement the same source may be located on a cell side or a cell corner. To ensure that locations of emission sources are tracked properly as the grid is moved, DSAGA-PPM includes appropriate logic. In this logic, the equation for each of the sides of a cell is derived using the coordinates of the pertinent grid nodes. Then starting with a grid cell, the location of a particular source is checked with respect to each side of the cell. If this check reveals that the source is within the cell, then the process is terminated. Otherwise such checks are performed with other cells to determine the source location. The process is repeated for any other sources present in the domain being modeled.

To solve the system of ordinary differential equations resulting from the application of the chemistry operator, DSAGA-PPM uses the *asymptotic integration method* of Young and Boris (1977). This method is self-starting and very fast, requires minimal storage, and produces reasonably accurate results at acceptable costs (McRae et al., 1982).

Further details on the numerical procedures for computation of transport, contribution of emission sources, and calculation of chemistry can be found in Srivastava et al. (2000) and Srivastava (1998).

2.2. Grid adaptation and solution correction

This adaptive grid algorithm is developed for use in a three-dimensional air quality model. It is general enough to be extended to three-dimensional applications. However, at least initially, a true need for a three-dimensional implementation of the algorithm is not envisioned. In the vertical direction, most air quality models (AQMs) use small grid spacing near the surface (e.g., 20 m) to resolve the boundary layer processes. The spacing is increased with altitude and, typically, 15–30 vertical layers are used from the ground up to the stratosphere. This usually provides sufficient vertical resolution. One situation where grid adaptation in the vertical may be beneficial is when there are convective clouds. On the other hand, there are situations (e.g., generation of photochemical smog) where clear skies lead to worse pollution episodes. For these latter situations, grid adaptation in the vertical may not be very useful. The need for adaptation in the horizontal direction is less arguable. There are large concentration gradients in the horizontal direction due to the sparse nature of pollutant sources. These gradients can be better captured by increased grid resolution. Considering these factors, grid adaptation in the horizontal direction is much more meaningful and, therefore, the DSAGA-PPM includes grid adaptation in the horizontal direction only.

In Sections 2.2.1–2.2.5 procedures for moving the grid nodes to the region(s) requiring solution refinement and for conservatively redistributing the solution field over the resulting adapted grid are described.

2.2.1. Weight function for flows with reacting species

In a flow with reacting species, these species may undergo complex dynamic transformations in time. Therefore, it may not be possible to predict a priori which of the species would dictate grid adaptation requirements in simulation of such a flow. Moreover, based on species concentrations, the active chemistry pathways in one part of the modeled region may be quite different from those active in other part(s). As a result, some of the species may need resolution in one part of the modeled region while other species may need resolution in other part(s). Further, these resolution needs may change with time. One possible strategy to ensure adequate grid adaptation in simulation of such a flow is to use a weight function that takes into account the resolution requirements of each of the species included in the chemical mechanism, at each time step in the simulation.

The SIERRA weight function formulation, developed by Laflin (1997), is easy to compute and promotes both grid node clustering and grid alignment adaptation processes. Using this formulation, a weight function for

use in grid adaptation may be expressed as

$$w_{i,j} = V_{i,j}^{1+e_1} \left| \left. \sum_{l=1}^{N} (\Delta^2 c_l) \right|_{i,j} + w_{\min} \right|, \qquad (11)$$

where $(\Delta^2 c_l)|_{i,j}$, represents the error at cell center i, j in the computed value of c_l with respect to the value obtained using interpolation of c_l values in the neighboring cells. In Eq. (11), the parameter e_1 controls the weighting of each cell volume V in relation to its size. If e_1 is negative, then smaller cells will be weighted more than larger cells and vice versa. Thus, choosing e_1 to be negative may cause smooth flow features to be under-resolved. In most cases, e_1 can be set to a value between -1.0 and -1.1. The parameter $w_{\min}$ is the minimum allowable weight function value and is typically set such that $10 \times$ machine zero $\leqslant w_{\min} \leqslant 1$. Larger values of $w_{\min}$ are chosen if grid adaptation is needed only in regions with prominent solution features. Note that values of both e_1 and $w_{\min}$ are provided by the user.

As defined in Eq. (11), the weight $w_{i,j}$ at cell center i, j would include information on the interpolation error at i, j in the computed concentration of each of the species l and, therefore, would be responsive to resolution needs of each of these species at i, j. However, in a flow with reacting species, the concentrations of these species may differ by several orders of magnitude. Therefore, each of the species-specific components $(\Delta^2 c_l)|_{i,j}$ in Eq. (11) needs to be scaled such that: 1) the interpolation error $(\Delta^2 c_l)|_{i,j}$ is relatively independent of the magnitude of c_l, 2) the scaled $(\Delta^2 c_l)|_{i,j}$ adequately represents the resolution requirements at i, j for each of the species l, and 3) the scaling process is responsive to the dynamic changes in species concentrations. Taking these requirements into consideration, a weight function suitable for use in simulations of reacting flows can be developed as follows.

Construction of the weight function with the above considerations starts with determination of the species-specific interpolation error at cell center i, j, given by a discrete approximation of the local Laplacian of c_l in unit-spaced curvilinear coordinates (Laflin, 1997):

$$(\Delta^2 c_l)|_{i,j} = \left| c_l|_{i-1,j} + c_l|_{i+1,j} + c_l|_{i,j-1} + c_l|_{i,j+1} - 4 \cdot c_l|_{i,j} \right|. \qquad (12)$$

The computed concentrations of various species would, in general, contain computational noise resulting from finite precision machine calculations. The effects of this noise need to be removed from the interpolation error given by Eq. (12), before this error is normalized and rescaled. In this work, the interpolation errors are adjusted to remove the computational noise. For each of the species, this adjustment involves normalizing the interpolation error at each cell center by the average value of the species concentration over the domain and setting the normalized value to zero in case this value is

less than or equal to 1×10^{-3}. The adjustment is shown below:

$$\overline{c_l} = \frac{\sum_{i,j} c_l|_{i,j}}{nn}, \quad nn = \text{number of grid cells}, \qquad (13)$$

$$\text{Adjusted}(\Delta^2 c_l)|_{i,j} = \frac{(\Delta^2 c_l)|_{i,j}}{\overline{c_l}}, \quad \forall \frac{(\Delta^2 c_l)|_{i,j}}{\overline{c_l}} > 1 \times 10^{-3},$$

$$= 0, \quad \forall \frac{(\Delta^2 c_l)|_{i,j}}{\overline{c_l}} \leqslant 1 \times 10^{-3}. \qquad (14)$$

The adjusted interpolation error given by Eq. (14) is further normalized using the maximum value over the domain as follows:

$$\text{Normalized}(\Delta^2 c_l)|_{i,j} = \frac{\text{Adjusted}(\Delta^2 c_l)|_{i,j}}{w_l^{\max}},$$

$$\text{Max } w_l = \text{MAX}[\text{Adjusted}(\Delta^2 c_l)|_{i,j}]. \qquad (15)$$

This latter normalization process scales the range of each $\text{Normalized}(\Delta^2 c_l)|_{i,j}$ to be between 0 and 1 and, therefore, satisfies the requirement 1) given above.

Note that the presence of a relatively large range in $(\Delta^2 c_l)$ over the entire grid would reflect that the spatial distribution of the concentration of species l requires significant resolution. Since the process of normalization given above compresses the range of each $(\Delta^2 c_l)$, it becomes necessary to restore each range by re-scaling.

First a linear combination of the normalized species-specific interpolation errors, $wc_{i,j}$, is formed at each cell center:

$$wc_{i,j} = \left. \sum_{l=1}^{N} \text{Normalized}(\Delta^2 c_l) \right|_{i,j}. \qquad (16)$$

Then this linear combination is re-scaled using

$$\text{Rescaled } wc_{i,j} = (wc_{i,j} - wc_{\min}) \frac{[(\Delta^2 c)_{\max} - w_{\min}]}{(wc_{\max} - wc_{\min})} + w_{\min}, \qquad (17)$$

where

$$wc_{\min} = \text{MIN}(wc_{i,j}), \quad wc_{\max} = \text{MAX}(wc_{i,j}) \qquad (18)$$

and

$$(\Delta^2 c)_{\max} = \text{MAX}(w_l^{\max}) \quad \forall l. \qquad (19)$$

The re-scaling scheme utilizing Eqs. (17)–(19) adjusts the range of values (maximum to minimum) of the Rescaled $wc_{i,j}$ to be between $w_{\min}$ and $(\Delta^2 c)_{\max}$. Since $(\Delta^2 c)_{\max}$ represents the largest interpolation error value for all species over the entire grid, this re-scaling scheme ensures that the resolution requirements of all species over the entire grid are represented in the weight function. Thus, requirement 2) above is satisfied. Further, the normalization and re-scaling process depends on time-dependent, species-specific

interpolation errors and, therefore, satisfies requirement 3) above.

Note that in Eq. (17), the lower end of the range of Rescaled $wc_{i,j}$ is fixed at $w_{\min}$. Consequently, $w_{\min}$ can be used to control the degree of adaptation (or the amount of grid movement).

Using the Rescaled $wc_{i,j}$, the weight function at a cell center i, j is given by (see Eq. (11))

$$w_{i,j} = V_{i,j}^{1+e_1} \left| \text{Rescaled } wc_{i,j} \right|. \tag{20}$$

The weight function resulting from Eq. (20) may result in highly sheared or skewed grids in which large cell volumes may exist next to small cell volumes. These large volumes can adversely affect the accuracy of solution calculations in the next time step. Hence, it is desirable to obtain smooth grids without highly sheared or skewed cells. Therefore, the weight function is smoothed using

$$w'_{i,j} = \tfrac{1}{4}(w_{i,j-1} + 2w_{i,j} + w_{i,j+1}) \tag{21}$$

and

$$w_{i,j} = \tfrac{1}{4}(w'_{i-1,j} + 2w'_{i,j} + w'_{i+1,j}) \tag{22}$$

Generally 10 to 20 passes of smoothing are needed.

2.2.2. Repositioning of grid nodes

In DSAGA-PPM, the grid nodes are repositioned by a *center-of-mass* scheme, proposed by Eiseman (1987). In this scheme, a grid node is repositioned such that its position coincides with the center-of-mass of a local cluster of cells, with mass distribution over the grid being defined by the weight function. Using this scheme, the new position coordinates of grid node o are given by

$$\vec{P}_o^{\text{new}} = \frac{\sum_{i=1}^{4} w_i \vec{P}_i}{\sum_{i=1}^{4} w_i}. \tag{23}$$

In Eq. (23), $\vec{P}_i$, $i = 1, \ldots, 4$, are the position coordinates in physical space of the centers of the cells that are local to the grid node o and w_i, $i = 1, \ldots, 4$ are the weights associated with these cells.

2.2.3. Solution redistribution

In DSAGA-PPM, a solver-independent solution field redistribution procedure (Laflin, 1997) is employed. In this procedure, the solution field is fixed with respect to an inertial frame while a control volume, $\hat{\Omega}$, is allowed to move arbitrarily through the spatial domain. To describe the motion of $\hat{\Omega}$ through the inertially fixed solution field, a fictitious grid time, t_g, is introduced. The moving control volume is a function of grid time, $\hat{\Omega} = \hat{\Omega}(t_g)$, but is not a function of physical time, $\hat{\Omega} \neq \hat{\Omega}(t)$. Conversely, the solution field is a function of physical time, $c_l = c_l(t)$, but is not a function of grid time, $c_l \neq c_l(t_g)$. Using these concepts with the Reynolds transport theorem (Warsi, 1993), a *conservative interpolation equation* (CIE) applied to a two-dimensional

grid cell with four sides is obtained. This CIE is

$$(\bar{c}_l V)^{n_g+1} = (\bar{c}_l V)^{n_g} + \sum_{p=1}^{4} \left(\hat{V}_p \big|_{n_g}^{n_g+1} \right) \left(\hat{c}_{lp} \big|_{n_g}^{n_g+1} \right),$$

$$l = 1, \ldots, N, \tag{24}$$

where $\bar{c}_l = \bar{c}_l(t_g)$ is the average value of c_l over cell volume $V = V(t_g)$, $\hat{V}_p \big|_{n_g}^{n_g+1}$ is the volume swept by cell side p during movement between grid time levels n_g and $n_g + 1$, and $\hat{c}_{lp} \big|_{n_g}^{n_g+1}$ is the average value of c_l in $\hat{V}_p \big|_{n_g}^{n_g+1}$. Eq. (24) is used to compute the interpolated cell-averaged values for the dependent variables, $\bar{c}_l^{n_g+1}$, $l = 1, \ldots, N$.

2.2.4. Grid convergence

In this work, an iterative process is used to obtain adequately converged grid node positions. At any time, the following steps are taken in order: (1) weights are computed using the approach described above; (2) grid nodes are moved using Eq. (23); (3) the solution is redistributed as described above; and (4) grid convergence is checked. If the grid is converged within a specified tolerance, then the solution is advanced through a new time step; otherwise, weights are recomputed and the grid movement/solution redistribution procedure is repeated. In DSAGA-PPM, a limit, δ, is set on the maximum movement of grid nodes relative to the largest cell side in the starting Cartesian grid such that

$$\frac{\text{MAX}\left| \Delta \vec{X}_{i,j} \right|}{\text{MAX}(\Delta x, \Delta y)_{\text{starting Cartesian grid}}} \leq \delta \quad \forall i,j, \tag{25}$$

where $\Delta \vec{X}_{i,j}$ is the change in position coordinates of the node i, j. If Eq. (25) is satisfied, then the grid is considered to be converged.

2.2.5. Preadaptation

In an air quality simulation, the domain being modeled, in general, will contain regions with relatively large gradients in species concentrations. Such gradients may result from complex interactions between emissions from sources, meteorological conditions, and atmospheric chemistry. A DSAGA-PPM simulation of this domain would start with a uniform distribution of grid nodes and would modify this distribution based on the spatial resolution requirements of the various species. However, using the starting uniform grid with initial gradients in species concentration can result in an inaccurate calculation of the solution field in the first time step. In order to avoid this possibility, a preadaptation step has been included in the DSAGA-PPM algorithm. In this step, the starting uniform grid is preadapted to regions with initial concentration gradients before calculating the solution field in the first time step. In general, this preadaptation is accomplished by

computing weights based on the initial solution field, moving the grid nodes, checking grid convergence, and stopping the preadaptation process once the grid is converged, as described in Sections 2.2.1–2.2.4. There could, however, be situations in which the initial solution field may not contain any concentration gradients, but sources in the domain start emitting at the beginning of the first time step. In such situations, emissions from sources are assumed to occur before the first time step; preadaptation process is completed based on the gradients resulting from these emissions, and then the solution field is reinitialized with background concentrations.

Note that in DSAGA-PPM, grid adaptation is carried out based on a user-selected multiple of time step. Thus adaptation can be carried out every time step or every Qth time step, where Q is an integer. A value of 4 for Q has been used in the simulations conducted thus far (Srivastava et al., 2000, Srivastava, 1998). Note also that the user needs to select values of cell volume weighting parameter e_1, the minimum allowable weight function value w_{min}, the number of smoothing passes, and the grid convergence parameter δ. These values are selected based on the experiments conducted to obtain an acceptable preadapted grid with nodes clustered around any solution field features, prior to taking the first time step in a simulation.

As discussed above, DSAGA-PPM automatically repositions the grid nodes to better resolve solution features. However, there is a limitation of the method related to the proximity of the features to the domain boundaries. In DSAGA-PPM the boundary nodes are not allowed to move inward, but can move only along the boundaries. Consequently, only limited resolution of features near the boundaries would be possible. Therefore, in general, it would be necessary to choose a domain whose boundaries are not too close to areas with large gradients in pollutant concentrations. Such areas may either exist as emission sources or may develop as a result of evolving solution features (e.g., power plant plumes). Choosing such a domain and starting grid will ensure that during the simulation adequate number of grid nodes are available on all sides of the solution field features needing resolution.

3. Description of the model problem and simulation conditions

In the model problem, a point source (i.e., a power plant) is located at coordinates (55, 105 km) in a two-dimensional region that is 210 km long in each of the x- and y-directions. The domain is initially discretized with 22×22 grid nodes, spaced uniformly. Thus, each cell in the initial uniform grid is a square with a side of 10 km. As discussed in Gillani and Pleim (1996), the current air quality models typically use grid cell sizes larger than $10 \times 10 \, km^2$. Therefore, in the context of contemporary air quality modeling, the grid chosen for the test case would be considered to be a refined grid. The transport parameters consist of a constant wind speed of 5 m/s in the x-direction and a constant horizontal turbulent diffusivity of $100 \, m^2/s$ for all species, in both the x- and y-directions. Note that the chosen value of diffusivity is consistent with the range of 50–100 m^2/s provided in Seinfeld (1986). Gillani and Pleim (1996) have reported that plumes from large power plants achieve spreads of 30–40 km as they travel downwind. The chosen value of diffusivity ensured that the plume spread in this test case is consistent with this finding.

Following Odman and Russell (1991), a simple chemical mechanism describing production and destruction of tropospheric O_3 is used in this work. This mechanism is shown in Table 1. The solar zenith angle, θ, that appears in the photolysis reactions of Table 1, is held constant at $71.5°$. This value corresponds to the average zenith angle experienced during an equinox day at the equator (Odman and Russell, 1991).

Note that, for this simplified chemical mechanism, the volatile organic compounds (VOCs) are lumped hydrocarbons (HCs) and formaldehyde (HCHO). Also NO_x is simply the mixture of nitric oxide (NO) and nitrogen dioxide (NO_2). As Per Gillani and Pleim (1996), the regional background in the Eastern US, in the summer daytime mixing layer, is typically characterized by relatively high VOC/NO_x ratios (~ 10–100). Moreover, Sillman et al. (1990) have used a NO_x concentration of 0.2 ppb in their simulations of urban and power plant plumes. Accordingly, for the model problem the background NO_x concentration and VOC/NO_x ratio are chosen to be 0.2 ppb and 35, respectively. These values correspond to a background VOC concentration of 7 ppb. For the cell containing the source (power plant), the VOC/NO_x ratio, consisting of

$$\frac{VOC_{background}(ppb) + VOC_{powerplant}(ppb)}{NO_{x_{background}}(ppb) + NO_{x_{powerplant}}(ppb)}$$

Table 1
A simplified chemical mechanism for production of ozone

Reaction	Rate
$HC + OH \rightarrow 4RO_2 + 2HCHO$	$k_1 = 6.0 \times 10^{-12}$
$HCHO + hv \rightarrow 2HO_2 + CO$	$J_2 = 7.8 \times 10^{-5} \, e^{-0.87}/\cos\theta$
$RO_2 + NO \rightarrow NO_2 + HCHO + HO_2$	$k_3 = 8.0 \times 10^{-12}$
$NO + HO_2 \rightarrow NO_2 + OH$	$k_4 = 8.3 \times 10^{-12}$
$NO_2 + hv \rightarrow NO + O_3$	$J_5 = 1.0 \times 10^{-2} \, e^{-0.39}/\cos\theta$
$NO + O_3 \rightarrow NO_2 + O_2$	$k_6 = 1.6 \times 10^{-14}$
$O_3 + hv \rightarrow O_2 + O \, (1d)$	$J_7 = 1.9 \times 10^{-4} \, e^{-1.9}/\cos\theta$
$O \, (1d) + H_2O \rightarrow 2OH$	$k_8 = 2.3 \times 10^{-11}$
$NO_2 + OH \rightarrow HNO_3$	$k_9 = 1.0 \times 10^{-11}$
$CO + OH \rightarrow CO_2 + HO_2$	$k_{10} = 2.9 \times 10^{-13}$

is chosen to be 0.3, which is less than the characteristic value of 1.0 for power plant plumes (Sillman et al., 1990). Further, Sillman et al. (1990) have reported that in the St. Louis region in the Eastern US, on average, the ratio of VOC to NO_x emissions from power plants is about 14%. This ratio is used in this model problem. Again, in accordance with Sillman et al. (1990), the ratios of

$$\frac{NO_{background}(ppb)}{NO_{2_{background}}(ppb)},$$

and

$$\frac{HCHO_{background}(ppb)}{VOC_{background}(ppb)}$$

are assumed to be 0.1 and 0.05, respectively. Finally, 10% of the power plant NO_x emission is assumed to be NO_2, the remaining 90% being NO. With these assumptions, the concentrations (molecules/cm^3) of VOC and NO_x emissions from the source are shown in Table 2. Further, using these concentrations, the chosen grid and transport parameters and a summer daytime mixing layer height of 1 km, the source terms (molecules/s) corresponding to NO_x and VOC emission rates from the power plant are calculated. These rates are also shown in Table 2.

The initial conditions for species other than VOCs and NO_x consist of the background concentrations based on Odman and Russell (1991). The initial conditions for all species are summarized in Table 2. Note that in the simulation, at time $= 0$ s, the power plant starts to emit NO_x and VOCs at the steady rates shown in Table 2.

For the model test problem presented here, results were obtained using DSAGA-PPM and the corresponding Static Grid Algorithm-PPM (SGA-PPM). These results are compared to reveal the advantages of using DSAGA-PPM. Note that SGA-PPM is obtained by deactivating the grid adaptation procedures in DSAGA-PPM. An SGA-PPM application utilizes a uniformly spaced grid that is identical to the starting grid used in the corresponding DSAGA-PPM application.

Each of the SGA-PPM and DSAGA-PPM simulations was carried out for 40,000 s (i.e., about 11 h) of daytime. In these simulations the CFL was set at 0.8. In the DSAGA-PPM simulation, the grid was adapted every fourth time step and the values of the grid adaptation related parameters were set as follows: e_1, w_{min}, and the number of smoothing iterations were set at -1.1, 1×10^{-1}, and 20, respectively; the value of the grid convergence parameter, δ, was set at 1.5×10^{-2}. The values of the adaptation parameters were determined through numerical experiments and were selected to obtain a good starting (preadapted) grid. This grid is shown in Fig. 1.

Table 2
Initial concentrations and source terms for the power plant plume model problem

Species	Initial concentration (molecules/cm^3)	Source (molecules/cm^3)	Source (molecules/s)
CO	1.00E+12		
H$_2$O	2.50E+15		
HC	1.64E+11	1.42E+11	8.87E+24
HCHO	8.61E+09	7.47E+09	4.67E+23
HO$_2$	1.00E+06		
NO	4.47E+08	9.60E+11	6.00E+25
NO$_2$	4.47E+09	1.07E+11	6.67E+24
O (1d)	1.00E-03		
O$_3$	5.00E+11		
OH	1.00E+05		
RO$_2$	1.00E+06		

4. Simulation results

The NO solution fields obtained using SGA-PPM and DSAGA-PPM, are shown in Figs. 2 and 3, respectively. A comparison of these figures reveals that the DSAGA-PPM solution, as expected, is less dispersed than the corresponding SGA-PPM solution. Further, the NO contour values in the DSAGA-PPM solution are higher than those in the SGA-PPM solution. In the SGA-PPM simulation, the source emissions are dispersed over a large grid cell volume and result in lower NO contours.

The regional nature of the O$_3$ plume can be seen in Figs. 4–7. In each of these figures starting from the source, the plume traverses regional scale distances. Further, Figs. 4 and 5 depict different spatial distributions of O$_3$, thereby indicating that grid cell size has a significant impact on the calculated O$_3$ field.

As seen in Fig. 7, the concentration of O$_3$ close to the source is much lower than the background. In the area close to the source (*the high-NO_x regime*), the chemistry is limited by the supply of odd-H radicals (OH, HO$_2$, and RO$_2$) relative to NO_x and, therefore, the oxidizing capacity of this environment is low. Consequently, O$_3$ is quickly depleted by the high levels of NO_x present near the source, according to the reaction:

$$NO + O_3 \rightarrow NO_2 + O_2. \tag{26}$$

As the O$_3$ plume travels downstream, the NO_x concentration decreases and turbulent diffusion causes the plume to gradually mix with the background HCs and HCHO. Consequently, the supply of odd-H radicals, relative to NO_x, increases. At some point in time, the chemistry in the plume shifts to a *low-NO_x regime* in which the supply of odd-H radicals, relative to NO_x, becomes large enough to cause an oxidizing environment in which NO is oxidized to NO_2 by the
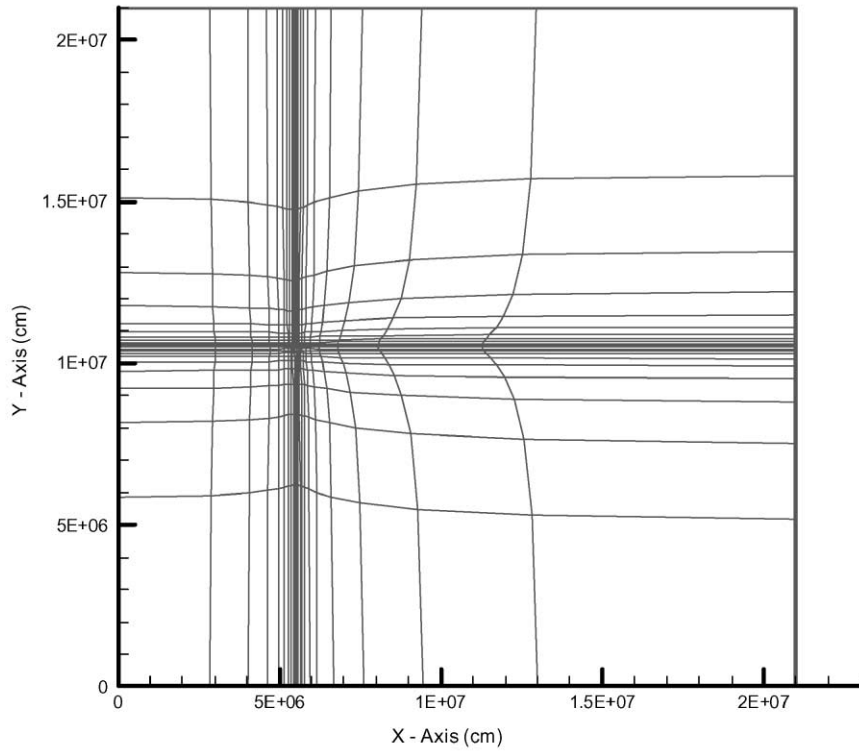
Fig. 1. Preadapted grid reflecting clustering of nodes near the point source.
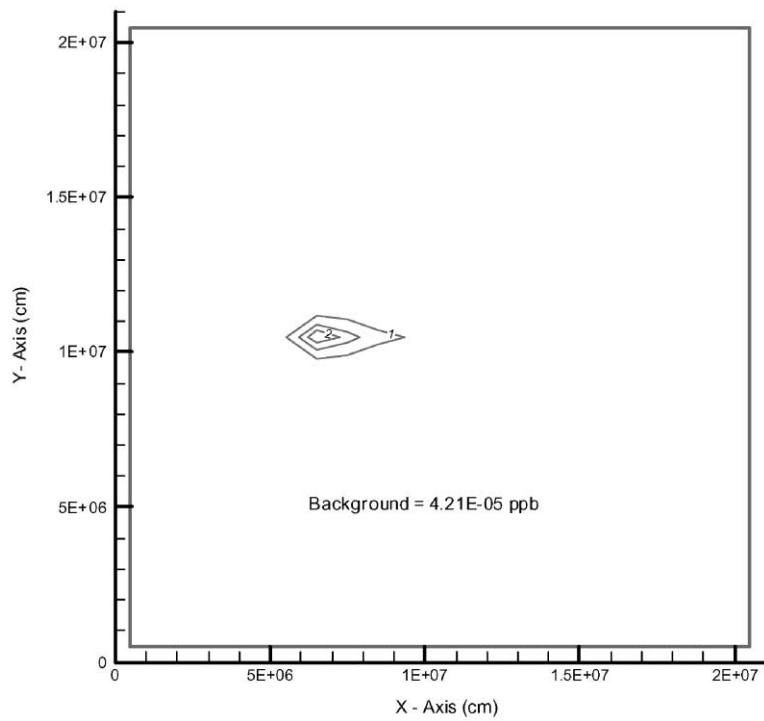
Fig. 2. SGA-PPM prediction of NO concentration after 40,000 s.
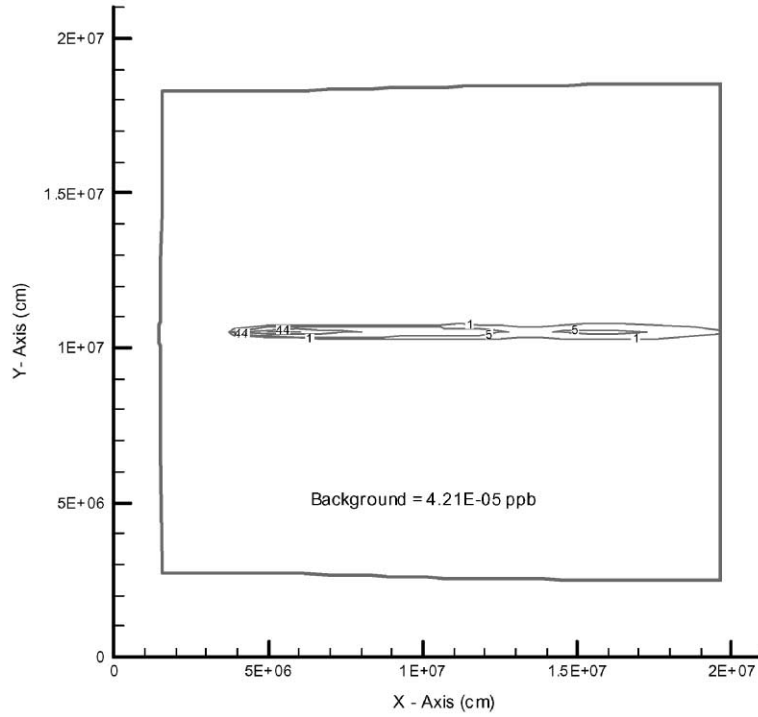
Fig. 3. DSAGA-PPM prediction of NO concentration after 40,000 s.
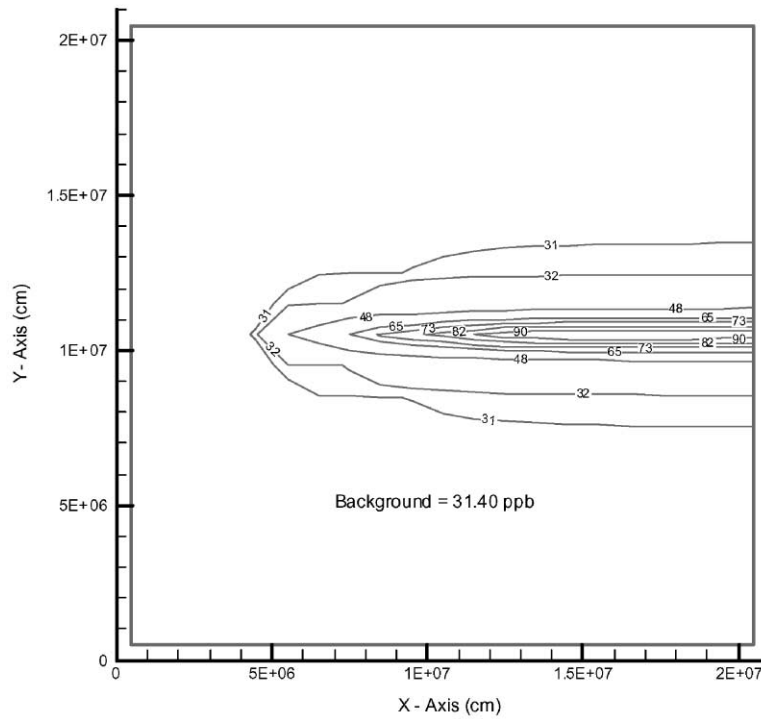
Fig. 4. SGA-PPM prediction of O$_3$ concentration after 40,000 s.

Fig. 5. DSAGA-PPM prediction of O_3 concentration after 40,000 s.

Maximum = 99.02 ppb

Minimum = 31.40 ppb

Background = 31.40 ppb
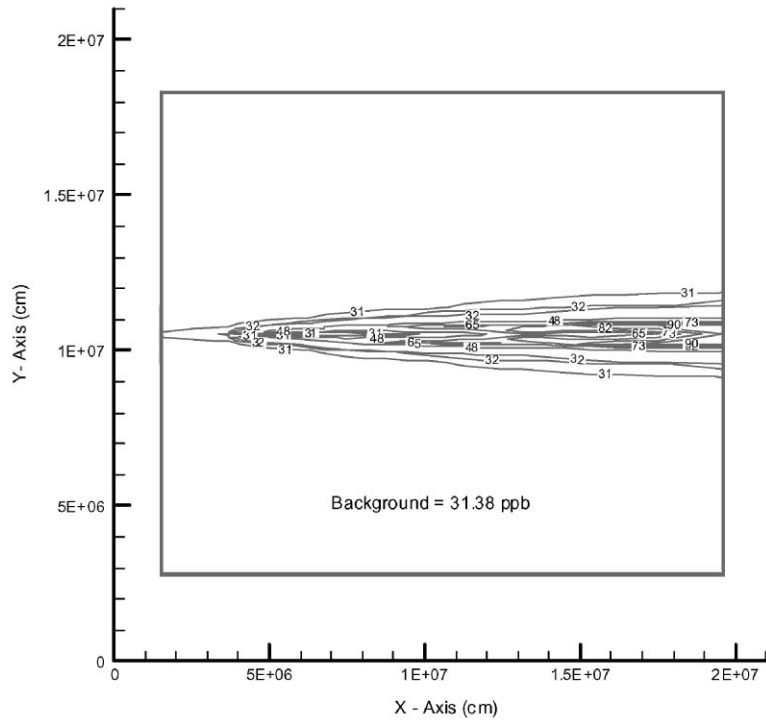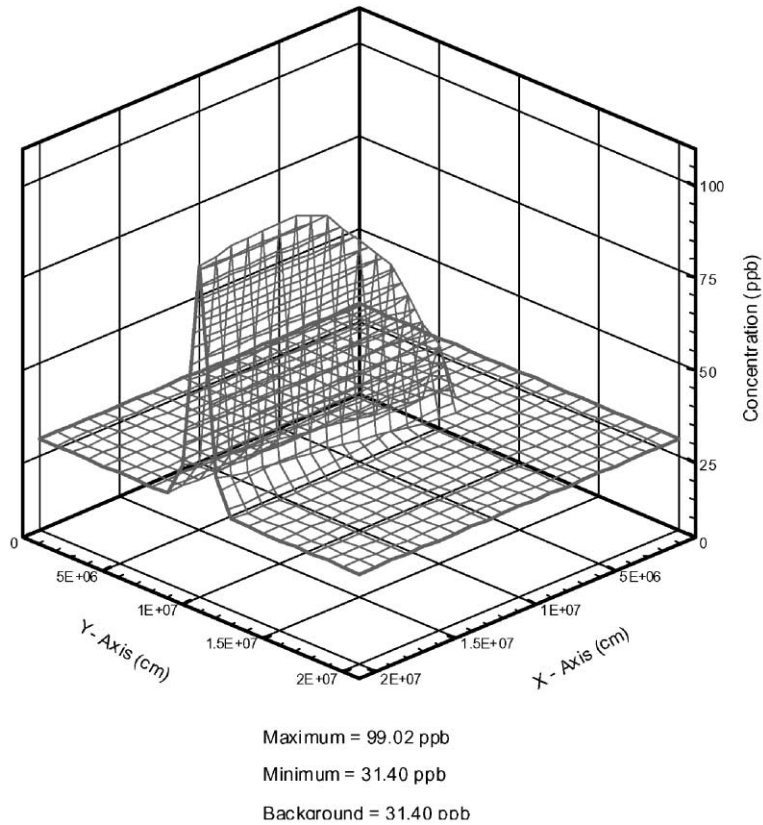
Fig. 6. Three-dimensional depiction of SGA-PPM results for O_3 concentration at 40,000 s.

Maximum = 103.92 ppb

Minimum = 14.02 ppb

Background = 31.38 ppb
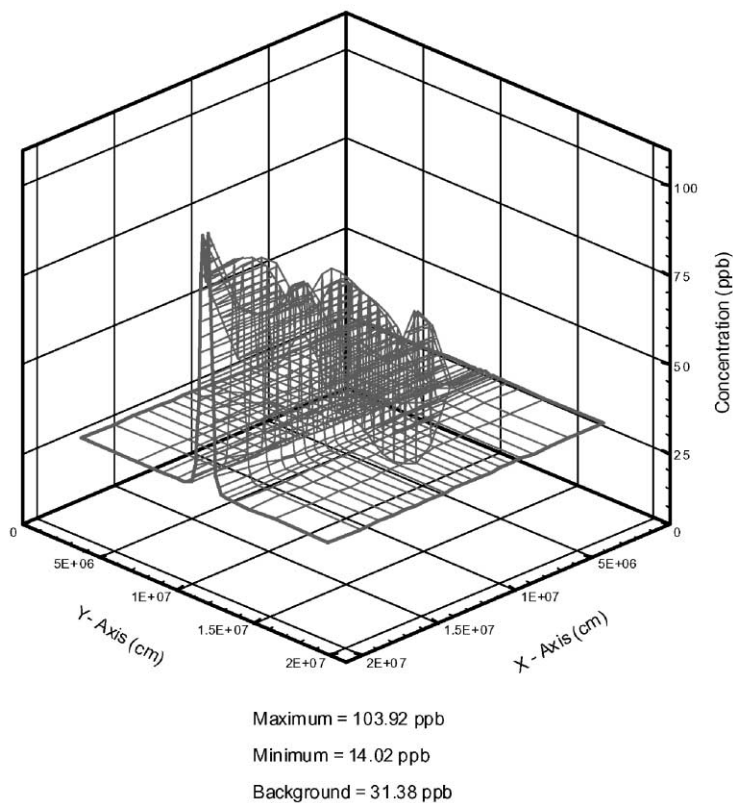
Fig. 7. Three-dimensional depiction of DSAGA-PPM results for O_3 concentration at 40,000 s.

odd-H radicals. This oxidation of NO competes with reaction (26) for the availability of NO and results in reduced destruction of O_3. The concentrations of O_3, therefore, rise above the background levels at quite large distances downwind of the source. This behavior is exhibited by the DSAGA-PPM solution presented in Fig. 7, but not by the SGA-PPM solution shown in Fig. 6. In the SGA-PPM simulation, power plant emissions are instantaneously dispersed over a large grid volume and their chemistry is artificially and suddenly shifted from that of the high-NO_x regime to low-NO_x regime. Consequently, the oxidation of NO to NO_2 and production of O_3 occur near the source.

The SGA-PPM and DSAGA-PPM O_3 concentrations in the plume cross-sections at distances of 10, 60, and 135 km from the source, are presented in Figs. 8(a, b, c), respectively. The DSAGA-PPM O_3 concentrations in these three plots represent the three general stages of plume chemistry, denoted as the "early", the "intermediate", and the "mature" stages (Gillani and Pleim, 1996).

In the "early" stage shown in Fig. 8(a), the plume chemistry is in the high NO_x regime described above

and, consequently, O_3 is depleted. As the plume travels downwind, its edges receive NO_x by diffusion from the plume core and VOCs and odd-H by entrainment from the background. These conditions become favorable for the generation of odd-H and, consequently, for the formation of O_3. Thus O_3 bulges develop at the plume edges. This is shown in the "intermediate" stage shown in Fig. 8(b). Finally, in the "mature" stage shown in Fig. 8(c), the plume volume is highly oxidizing and substantial excess of O_3 over background occurs. Such stages were observed in the measurements made on the Labadie Power Plant plume, as noted in Gillani and Pleim (1996). Note that the SGA-PPM O_3 concentrations in the plume shown in these figures do not exhibit the expected near-source plume structure. This reflects that the SGA-PPM application is unable to resolve the delicate and nonlinear nature of NO_x and odd-H chemistry.

The DSAGA-PPM solution fields for O_3 at 3600 and 10,800 s are shown in Figs. 9 and 10. The results in these figures depict the evolution of the O_3 solution field in time. At 3600 s, the O_3 valley near the source is much deeper than that at 10,800 s, reflecting the initial rapid
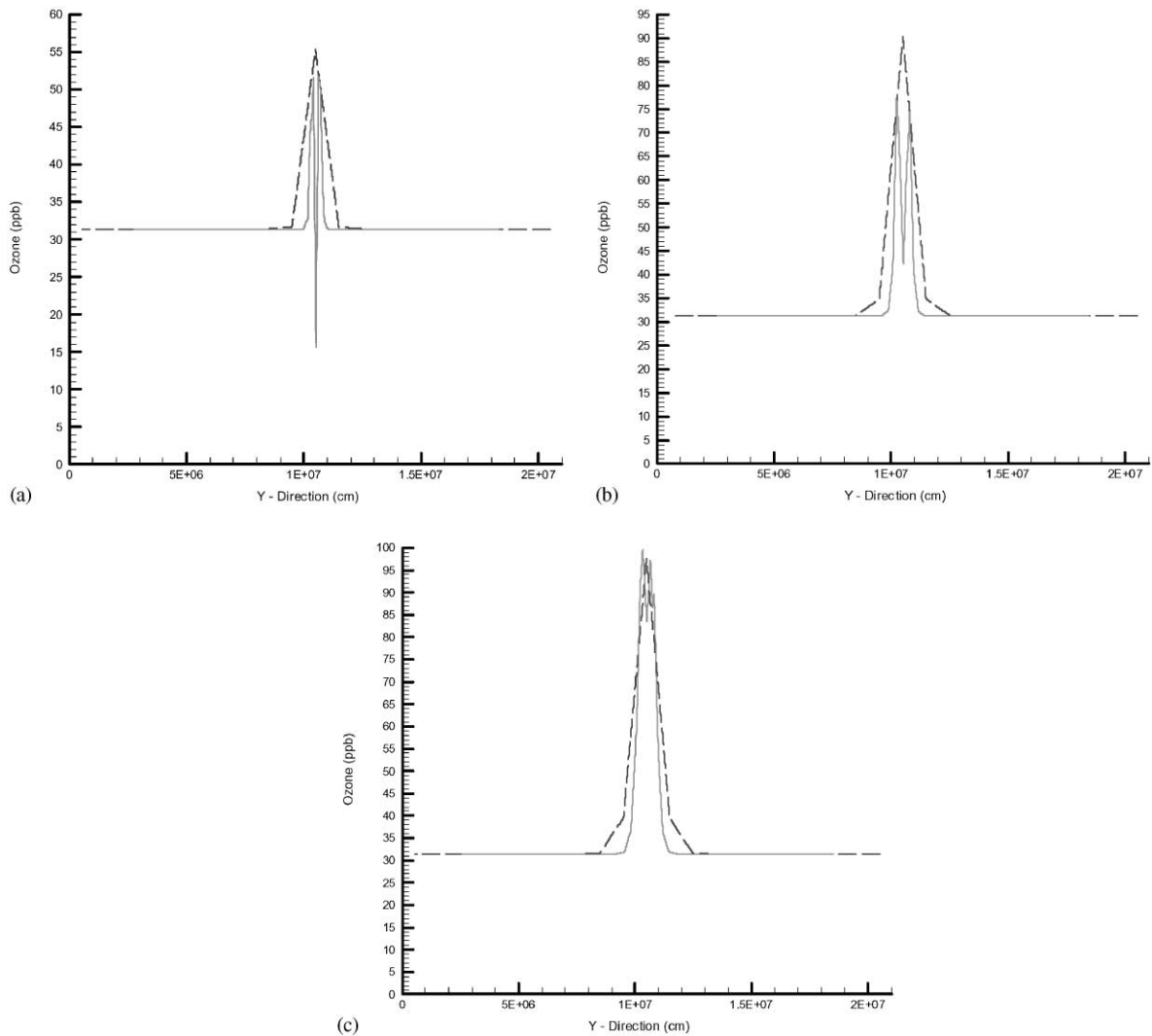
Fig. 8. SGA-PPM and DSAGA-PPM predictions of O_3 concentration in plume cross-section at a distance of (a) 10 km downwind of the source, (b) 60 km downwind of the source, and (c) 135 km downwind of the source. SGA concentrations are depicted by the dashed curves.

depletion of background O_3 concentration. This consumption of O_3 occurs via production of NO_2 (see reaction (26)), which, in turn, leads to some O_3 production through photochemistry. Thus, in the simulation some O_3 is produced at the source cell and some is transported to the source cell by turbulent diffusion. As the simulation progresses in time, O_3 concentration in the source cell, as well as other cells, increases due to photochemistry. Consequently, the O_3 valley near the source becomes shallower in time. These results demonstrate that DSAGA-PPM is able to resolve the varying temporal scales of O_3 solution field through dynamic grid adaptation.

The grid resulting from DSAGA-PPM simulation for 40,000 s is shown in Fig. 11. As seen in this figure, the grid nodes are clustered near the source and in the plume. Thus the grid appears to have responded to the resolution needs of the solution field.

In order to examine the mass conservation capability of DSAGA-PPM, the mass-balance of nitrogen (N) atoms was computed in each of the SGA-PPM and DSAGA-PPM simulations. The values of this balance are 99.97% for SGA-PPM and 99.96% for DSAGA-PPM. These results reflect that both SGA-PPM and DSAGA-PPM are able to maintain mass with a high degree of accuracy.

Maximum = 40.31 ppb

Minimum = 6.42 ppb

Background = 22.01 ppb
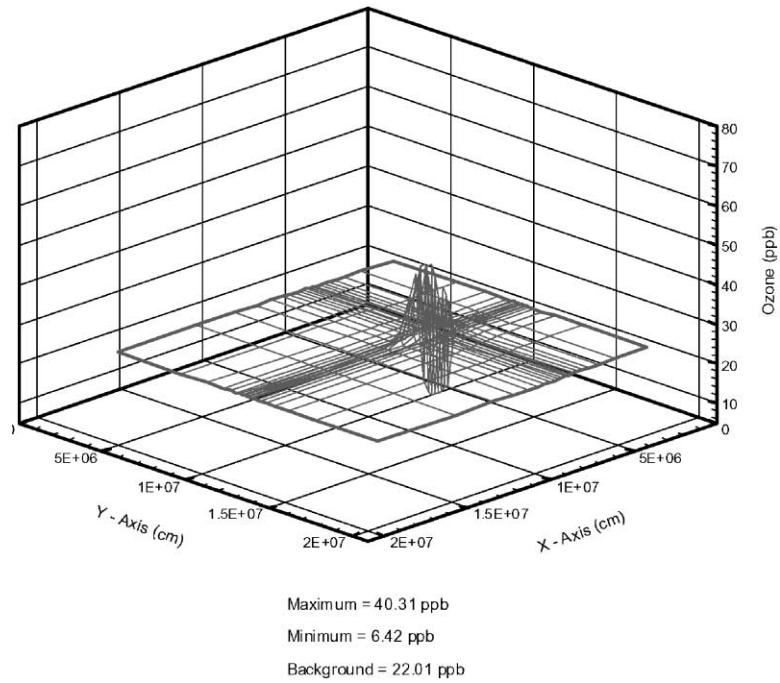
Fig. 9. DSAGA-PPM prediction of O_3 concentration field at 3600 s.

Maximum = 71.41 ppb

Minimum = 8.85 ppb

Background = 25.32 ppb
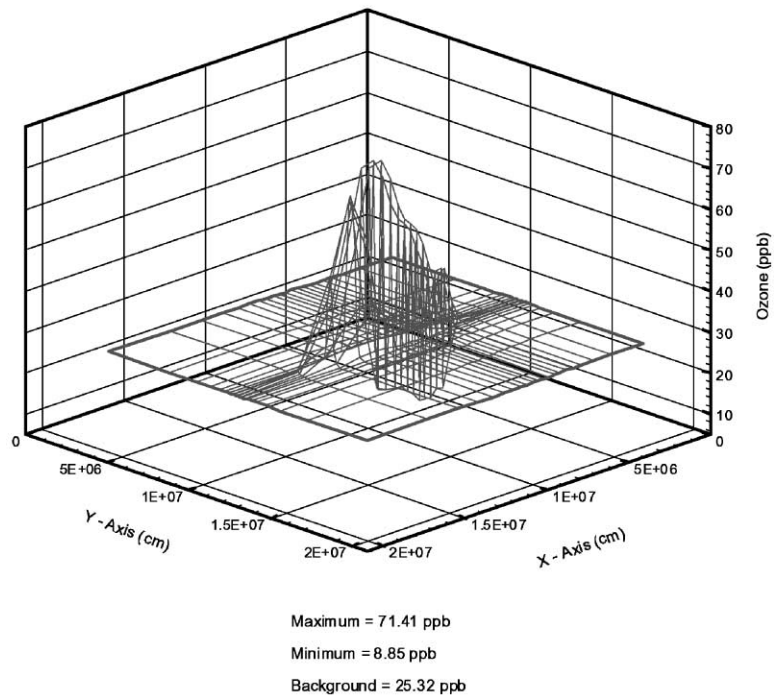
Fig. 10. DSAGA-PPM prediction of O_3 concentration field at 10,800 s.
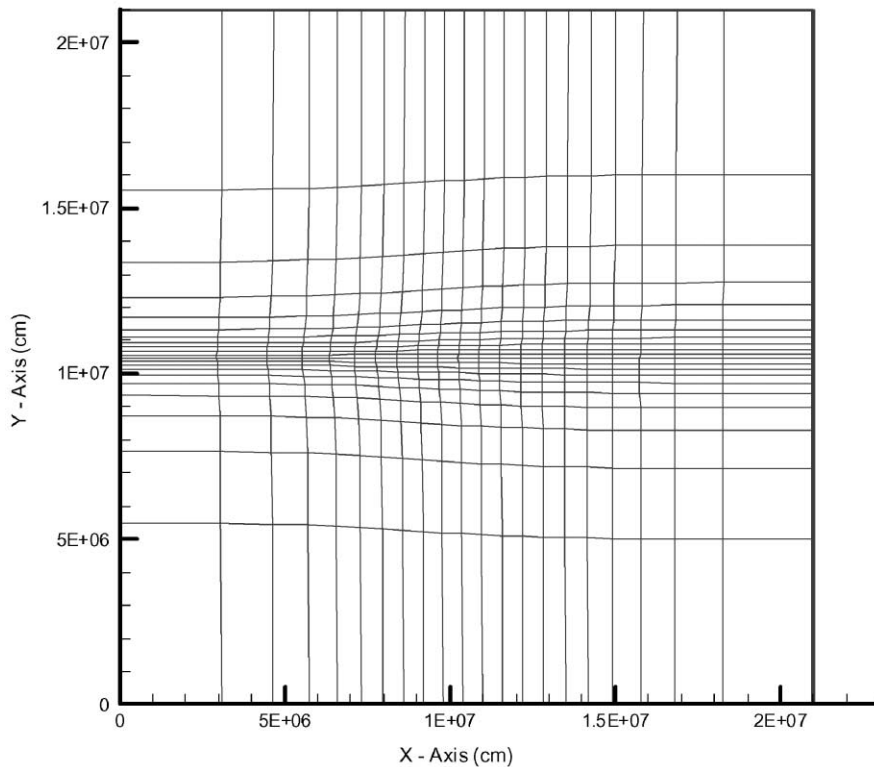
Fig. 11. Adaptive grid after 40,000 s reflecting clustering of nodes near the source and in the plume.

5. Assessment of the accuracy of DSAGA-PPM predictions

It is important to ensure that the DSAGA-PPM results obtained for this model problem are a reasonably accurate description of reality. The fact that the near-source plume structure captured by the DSAGA-PPM solution is consistent with the measured findings is reassuring. A comparison of this solution with a more accurate SGA-PPM solution may provide further assessment of its accuracy. Accordingly, a refined-grid SGA-PPM solution for 40,000 s, utilizing 110×110 grid nodes, was obtained for this model problem. Note that, with these nodes, the cell size in the refined grid is $3.68\,km^2$, which corresponds to the average of minimum cell sizes of 0.2 and $7.16\,km^2$ occurring during the DSAGA-PPM simulation.

Shown in Fig. 12 is the O_3 field resulting from the refined grid simulation. The O_3 valley in the vicinity of the source seen in this figure is consistent with the DSAGA-PPM result shown in Fig. 7. The O_3 concentrations in the plume cross-sections at distances of 10, 60, and 135 km from the source, respectively, obtained using the refined grid SGA-PPM and DSAGA-PPM are

presented in Figs. 13(a, b, c). As seen in these plots, the refined grid SGA-PPM solutions reflect the "early", the "intermediate", and the "mature" stages of plume development captured by the DSAGA-PPM solutions. These results indicate that the more accurate SGA-PPM solution obtained using a refined grid is equivalent to the DSAGA-PPM solution and, therefore, the adaptive grid solution is a reasonably accurate depiction of reality.

6. Computational performance

As discussed in the previous sections, a solution with a specific level of accuracy can be obtained using either DSAGA-PPM with relatively few grid nodes or a refined grid SGA-PPM with many more nodes. However, to assess the practicality of using DSAGA-PPM in air quality simulations, it is useful to obtain an indication of its computational performance. The model problem considered in this paper is of practical relevance and, therefore, is appropriate for an assessment of DSAGA-PPM's computational performance.

As discussed above, in this work SGA-PPM and DSAGA-PPM simulations were conducted using grids

Maximum = 110.40 ppb

Minimum = 10.79 ppb

Background = 31.38 ppb
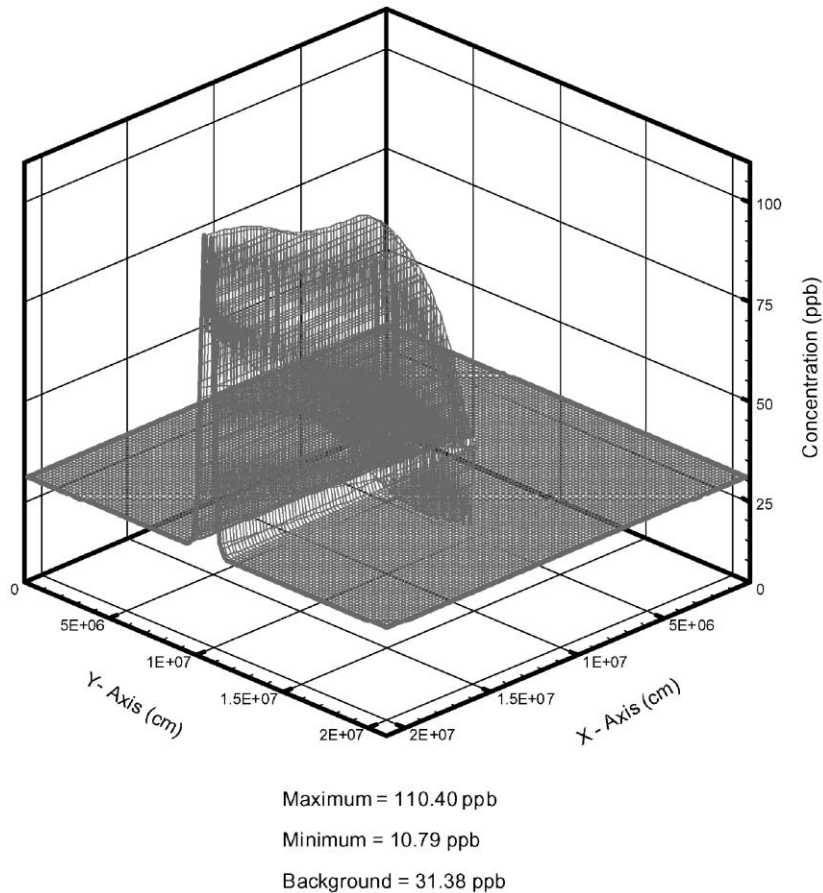
Fig. 12. Refined grid SGA-PPM prediction of O_3 concentration field at 40,000 s.

with 22×22 nodes, and a third simulation used SGA-PPM on a refined grid with 110×110 nodes. All these simulations were conducted on a CRAY T90 machine using a CFL of 0.8, and the code used performs at about 223 million floating-point operations per second for an average vector length of about 110 units. Note that, in the DSAGA-PPM simulation, the smallest cell size changed with time and ranged between 0.2 and 7.16 km^2.

The SGA-PPM solution over a 22×22 nodes static grid needed 210.4783 s of CPU time. However, as discussed above, this solution is less accurate than that obtained using DSAGA-PPM. In contrast, findings in Section 5 reflect that the refined grid SGA-PPM simulation resulted in a solution that is equivalent to the one obtained using DSAGA-PPM. However, this simulation used 3236.1376 s of time on the CRAY T-90 compared with 481.803 s needed to complete the DSAGA-PPM simulation. Thus, the refined grid SGA-PPM simulation took about 7 times more CPU time

than DSAGA-PPM simulation. While it is difficult to generalize these indications, the results do reflect that DSAGA-PPM has the potential to provide accurate air quality simulations at significant cost savings. In the near future, a more detailed assessment of DSAGA-PPM's performance would be deduced from realistic air quality simulations.

7. Conclusions

The potential for use of a dynamic solution adaptive grid algorithm (DSAGA-PPM) in air quality modeling has been investigated via application to a model problem, in which simplified photochemical production of O_3 occurs in a power plant plume. The results reflect that DSAGA-PPM is able to resolve the multiple spatial and temporal scales associated with O_3 production and transport. As such, DSAGA-PPM is able to resolve simultaneously both regional O_3 plume distribution and
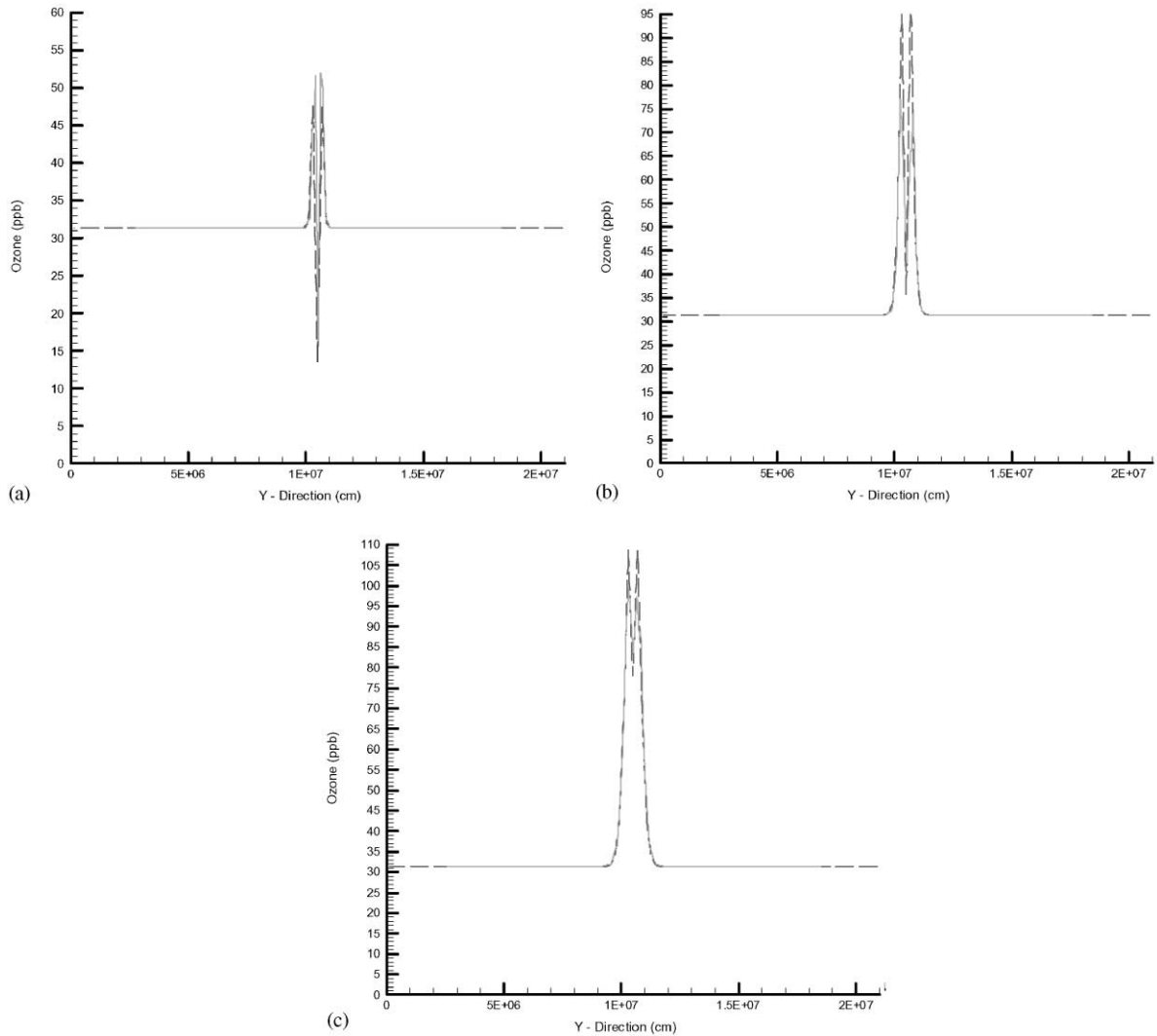
Fig. 13. Refined grid SGA-PPM and DSAGA-PPM predictions of O_3 concentration in plume cross-section at a distance of: (a) 10 km downwind of the source, (b) 60 km downwind of the source, and (c) 135 km downwind of the source. Refined grid SGA concentrations are depicted by dashed curves.

the small-scale plume structure near a source. In contrast, the small-scale plume structure is not resolved in the solution obtained using the corresponding static grid algorithm (SGA-PPM). In particular, concentration distributions near the source were incorrect in the low-resolution fixed-grid solution. Excellent mass conservation is exhibited in both DSAGA-PPM and SGA-PPM simulations.

Finally, a significant computational efficiency advantage may be possible if DSAGA-PPM is used in an AQM. Results for the model problem indicate that an SGA-PPM simulation using a refined grid with 110×110 nodes takes about 7 times more CPU time

than that needed by a DSAGA-PPM simulation on a grid with 22×22 nodes to provide a solution of equivalent accuracy. Therefore, it is concluded that DSAGA-PPM has the potential to greatly improve either AQM accuracy or efficiency, or a combination of both.

The capability of DSAGA-PPM to provide accurate solutions of coupled transport and nonlinear chemistry processes has been investigated in additional model problems. Currently, these results are being processed for future publication. In addition, efforts are underway to integrate DSAGA-PPM with a currently used AQM. Subsequently, a more detailed assessment of

DSAGA-PPM's performance would be deduced from realistic air quality simulations.

Disclaimer

The research described in this article has been reviewed by the US Environmental Protection Agency, and approved for publication. The contents of this article should not be construed to represent Agency policy.

References

Almgren, A.S., Bell, J.B., Colella, P., Howell, L.H., Welcome, M.L., 1997. A high resolution adaptive projection method for regional atmospheric modeling. In: Delic, Wheeler, (Eds.), Next Generation Environmental Models and Computational Methods. SIAM, Philadelphia, pp. 69–79.

Anderson, D.A., Tannehill, J.C., Pletcher, R.H., 1984. Computational Fluid Mechanics and Heat Transfer. Hemisphere Publishing Corporation, New York, pp. 252–255.

Carpenter, R.L., Droegemeier, K.K., Woodward, P.R., Hane, C.E., 1990. Application of the piecewise parabolic method (PPM) to meteorological modeling. Monthly Weather Review 118, 586–612.

Collela, P., Woodward, P.R., 1984. The piecewise parabolic method (PPM) for gas-dynamical simulations. Journal of Computational Physics 54, 174–201.

Dietachmayer, G.S., Droegemeier, K.K., 1992. Application of continuous dynamic grid adaption techniques to meteorological modeling. Part I: basic formulation and accuracy. Monthly Weather Review 120, 1675–1706.

Eiseman, P.R., 1987. Adaptive grid generation. Computer Methods in Applied Mechanics and Engineering. 64, 321–376.

Gillani, N.V., Pleim, J.E., 1996. Sub-grid scale features of anthropogenic emissions of NO_x and VOC in the context of regional Eulerian models. Atmospheric Environment 30, 2043–2059.

Laflin, K.R., 1997. Solver independent r-refinement adaptation for dynamic numerical simulations. Ph.D. Thesis. North Carolina State University, Raleigh, NC.

McRae, G.J., Goodin, W.R., Seinfeld, J.H., 1982. Numerical solution of the atmospheric diffusion equation for chemically reacting flows. Journal of Computational Physics 45, 1–42.

Odman, M.T., Russell, A.G., 1991. Multiscale modeling of pollutant transport and chemistry. Journal of Geophysical Research 96, 7363–7370.

Odman, M.T., Mathur, R., Alapaty, K., Srivastava, R.K., McRae, D.S., Yamartino, R.J., 1997. Nested and adaptive grids for multiscale air quality modeling. In: Delic, Wheeler, (Eds.), Next Generation Environmental Models and Computational Methods. SIAM, Philadelphia, pp. 59–68.

Seinfeld, J.H., 1986. Atmospheric Chemistry and Physics of Air Pollution. Wiley, New York, p. 598.

Sillman, S., Logan, J.A., Wofsey, S.C., 1990. A regional scale model for ozone in the united states with subgrid representation of urban and power plant plumes. Journal of Geophysical Research 95, 5731–5748.

Skamarock, W.C., Klemp, J.B., 1993. Adaptive grid refinement for two-dimensional and three-dimensional nonhydrostatic atmospheric flow. Monthly Weather Review 121, 788–804.

Srivastava, R.K., 1998. An adaptive grid algorithm for air quality modeling. Ph.D. Thesis. North Carolina State University, Raleigh, NC.

Srivastava, R.K., McRae, D.S., Odman, M.T., 2000. An adaptive grid algorithm for air quality modeling. Journal of Computational Physics 165, 437–472.

Tomlin, A., Berzins, M., Ware, J., Smith, J., Pilling, M.J., 1997. On the use of adaptive gridding methods for modelling chemical transport from multi-scale sources. Atmospheric Environment 31, 2945–2959.

Warsi, Z.U.A., 1993. Fluid Dynamics Theoretical and Computational approches. CRC Press, Boca Raton, p. 13.

Young, T.R., Boris, J.P., 1977. A numerical technique for solving stiff ordinary differential equations associated with the chemical kinetics of reactive flow problems. Journal of Physical Chemistry 81, 2424–2427.